Engineered Science
DOI: https://dx.doi.org/10.30919/es1868

Functionalization of Cellulose Nanofibers for Enhanced Immobilization of Recombinant Lipase in Palm Oil Hydrolysis

Ghusrina Prihandini,[1] Wilda Panjaitan,[1] Elvi Restiawaty,[1,2,3,4,*] Dian Ahmad Hapidin,[5] Akhmaloka Akhmaloka[6] and Yogi Wibisono Budhi[1,2,3]

Abstract

The utilization of cellulose nanofiber (CNF) as a support matrix for enzyme immobilization demonstrates significant promise for biocatalytic application. This research focuses on synthesis and stepwise functionalizing CNF using 3-aminopropyltriethoxysilane (APTES), glutaraldehyde, nitrilotriacetic acid (NTA), and nickel ions to achieve oriented immobilization of histidine-tagged (His-tagged) recombinant lipase ITB 1.2. The functionalization steps were systematically characterized to confirm the formation of specific chemical bonds. The effect of fiber diameter on enzyme immobilization efficiency was investigated, revealing an enzyme loading capacity of 21.53 mg/g after 24 hours. The immobilization yield reached 90.4% and 88% for CNFs with diameter of 660 nm and 800 nm, respectively. The corresponding catalytic activities were 94.41 U/mg and 104.81 U/mg. The immobilized enzyme was applied in a hydrolysis reaction using a rotating bed reactor at varying rotational speeds of 400, 500, and 600 rpm, resulting in hydrolysis efficiencies of 40%, 57%, and 63%, respectively.

Keywords: Cellulose nanofiber; Enzyme immobilization; Recombinant lipase; Rotating bed reactor; Nickel-functionalized support.
Received: 25 April 2025; Revised: 29 October 2025; Accepted: 10 November 2025
Article Type: Research article.

1. Introduction

The enzymatic hydrolysis of lipids using immobilized lipases has gained significant attention due to its potential for sustainable biocatalytic application. Lipase immobilizations offer several advantages including enhanced enzyme stability, reusability, and improved catalytic efficiency compared to free enzymes.[1] However, selecting an appropriate support material is crucial, as it directly influences the efficiency of immobilization, enzyme loading capacity, and overall reaction yield.[2] Previous studies have investigated various support matrices for lipase immobilization, such as non-porous cellulose nanocrystal (CNCs) and nickel-based materials. For instance, lipase immobilized on CNCs achieved a palm oil hydrolysis conversion rate of only 25–28%, likely due to limited enzyme-substrate interactions.[3,4] Conversely, lipase immobilization on nickel foam matrices, which possess pore sizes ranging from 7 to 20 nm, resulting in an immobilization efficiency of 97.45%.[5] While high porosity can enhance enzyme loading, excessive pore sizes increase the risk of enzyme leaching, reducing catalytic efficiency over time.[6,7]. Therefore, an optimal support matrix should balance structural stability, high surface area, and controlled porosity to achieve efficient and stable enzyme immobilization.

Cellulose, which is rich in hydrophilic hydroxyl groups, presents a highly attractive candidate for a wide range of applications due to its inherent biodegradability and biocompatibility, positioning it as one of the most promising natural materials.[8] The incorporation of nanoscale fibers, cellulose nanofibers (CNF) has emerged as a strategic and innovative approach in the fabrication of composite matrices, offering significant improvements in mechanical strength, surface area, tuneable porosity and interfacial interactions, which are critical for enhancing the overall performance and functionality of advanced materials. unique physicochemical properties, such as high surface.[9,10] Their highly porous network allows for enhanced enzyme substrate interactions, facilitating efficient catalytic activity and enzyme recovery. Additionally, CNF membranes provide a biocompatible environment for enzyme immobilization, reducing enzyme denaturation and improving operational stability.

CNF generated either by top-down or bottom-up approach methods. The top-down approach means generating fiber from expose complex natural resources into simplified. Meanwhile,

[1]*Department of Chemical Engineering, Institut Teknologi Bandung, Jl. Ganesha 10, Bandung, West Java, 40132, Indonesia*
[2]*Research Centre for Nanoscience and Nanotechnology, Institut Teknologi Bandung, Jl. Ganesha 10, Bandung, West Java, 40132, Indonesia*
[3]*Research Group of Chemical Engineering Process Intensification, Institut Teknologi Bandung, Jl. Ganesha 10, Bandung, 40132, Indonesia*

bottom-up approaches define as generating small molecule material convert into complex structure or generation of novel nanofiber structures. Several bottom-up methods were conduct to fabric CNF membranes including electrospinning,[11] layer by layer (LBL) self-assembly.[12] Among the diverse fabrication techniques, electrospinning has gained prominence as a direct and efficient method for generating continuous nanofibers with uniform diameters, enabling large-scale production within a relatively short processing duration.[11,13] Typically, the electrospinning technique employs cellulose solution that originates from solid-phase cellulose nanoparticles.[14]

To further enhance enzyme stability and catalytic efficiency, surface modification of CNFs is necessary. Functionalization with 3-aminopropyl triethoxysilane (APTES) introduce amine groups, which facilitate covalent attachment of crosslinkers such as glutaraldehyde, enabling stronger enzyme-matrix interaction.[15] Previous study have shown that lipase immobilized on unmodified CNFs exhibited an enzyme activity of 29.6 U/g under operational conditions of 25–35 °C and pH 5.5–6.5.[15] Further modification incorporating glutaraldehyde and pentaethylenehexamine as spacer arms improved enzyme retention, achieving an enzyme loading of 28.9 mg/g and a hydrolysis activity of 44.3% under optimized conditions.[16] In another study, lipase was immobilized using glutaraldehyde within electrospun nanofibers composed of graphene oxide, chitosan, and cellulose acetate, successfully retaining 80% immobilization.[17]

A more advanced immobilization strategy involves the use of nitrilotriacetic acid (NTA) combined with nickel ions, enabling oriented immobilization of His-tagged enzymes. NTA exhibits strong affinity for divalent metal ions, such as Ni^{2+} and Co^{2+}, which form stable coordination complexes with proteins containing histidine residues.[18] These metal-ligand interactions enhance enzyme stability and activity by preserving the structural conformation of the active site.[19] Compared to copper, which can only immobilize protein with a single histidine, nickel and cobalt require at least two histidine residues, leading to stronger and more stable enzyme binding.[20] Additionally, nickel-functionalized supports have demonstrated superior enzyme retention and reusability in various catalytic systems.[21]

In this study, a novel thermostable recombinant lipase ITB 1.2, derived from the local isolate *Geobacillus thermoleovorans* PPD 2,[22] was immobilized onto a functionalized CNF matrix. This recombinant lipase contains an imidazole ring that enhances its compatibility with nickel-based supports, further improving its stability and catalytic performance.[23] The enzyme exhibits optimal activity at 60 °C and pH 9.0, making it well-suited for industrial application requiring high-temperature stability.

To address challenges related to mass transfer limitations and inefficient substrate-enzyme interactions, a Rotating Bed Reactor (RBR) was employed in this study. Traditional immobilization methods often suffer from poor dispersion, low mass transfer rates, and broad particle size distribution, which hinder catalytic efficiency.[24] RBR technology offers enhanced mixing and mass transfer characteristics, leading to improved reaction kinetics and higher conversion rates.[25] By integrating immobilized CNF-supported lipase within an RBR system, this study aims to achieve a more efficient and scalable approach for lipid hydrolysis.

This research presents a systematic approach to the synthesis, functionalization, and characterization of CNF-based supports for recombinant lipase immobilization. Furthermore, the performance of the immobilized recombinant lipase ITB 1.2 was evaluated in a hydrolysis reaction within RBR system, demonstrating its potential for high-efficiency biocatalyst in industrial applications.

2. Material and methods

2.1 Materials

Cellulose acetate (CA) with an acetyl content of 39.8% was utilized without further purification. Recombinant ITB 1.2 lipase from *Geobacillus thermoleovorans* PPD2 was expressed in *Escherichia coli*, yielding an activity of 60.38 U/mL. The following reagents were used in this study: Bradford reagent, bovine serum albumin (BSA), *p*-nitrophenyl palmitate (*p*-NPP), glutaraldehyde, *nitrilotriacetic acid* (NTA), and nickel chloride. All chemicals were purchased from Sigma-Aldrich Chemical Co., and other reagents were of analytical grade and used without further purification.

2.2 Nanofiber synthesis

A solvent mixture of acetone and *N,N*-dimethylacetamide (DMAc) in a 3:2 mass ratio was prepared. A homogeneous 15 % (w/w) cellulose acetate (CA) solution was obtained by dissolving CA in this solvent for 2 hours. Before injection, the solution was ensured to be free of air bubbles and then loaded into a 20 mL syringe fitted with a 0.7 mm inner diameter metal needle connected to a high-voltage power supply. The nanofiber membrane was fabricated via electrospinning method. An ILMI-N101 electrospinning apparatus was operated at a potential of 17 kV, with a 15 cm distance between the needle tip and a square aluminium ground. The solution feed rate was maintained at 0.5 mL/hr using a syringe pump, as illustrated in Fig. 1 (a). To achieve sufficient membrane thickness for further processing and modification, electrospinning was conducted for 40 hours.

The cellulose acetate (CA) nanofiber membrane was

[4]*Bioenergy Engineering and Chemurgy Institut Teknologi Bandung, Jl. Ganesha 10, Bandung, West Java, 40132, Indonesia*
[5]*Physics and Technology of Advanced Materials, Faculty of Mathematics and Natural Sciences, Institut Teknologi Bandung, Jl. Ganesha 10, Bandung, West Java, 40132, Indonesia*
[6]*Biochemistry and Biomolecular Engineering Research Group, Faculty of Mathematics and Natural Sciences, Institut Teknologi Bandung, Jl. Ganesha 10, Bandung, West Java, 40132, Indonesia*
[*]*Email:* e.restiawaty@itb.ac.id (Elvi Restiawaty)

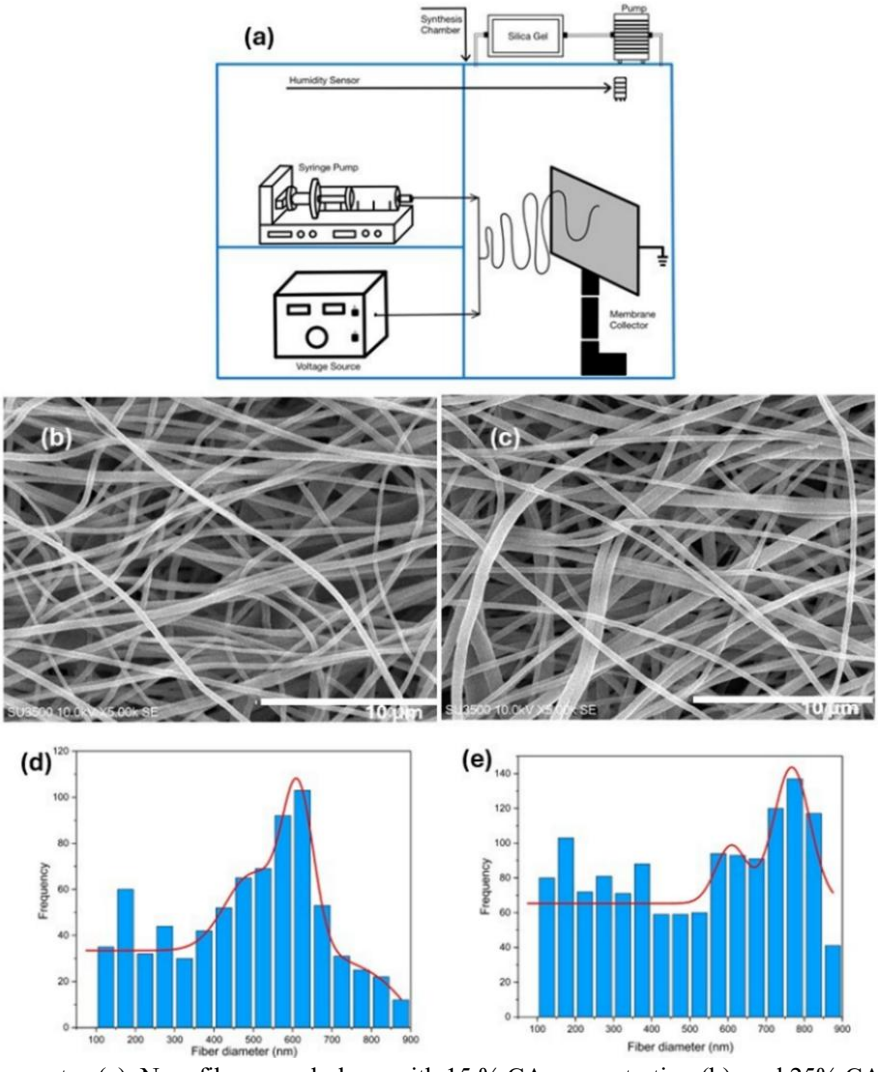

Fig. 1: Electrospinning apparatus (a), Nanofiber morphology with 15 % CA concentration (b), and 25% CA concentration (c), along with its fibers diameters for 15% concentration (d), and 25% concentration (e).

converted into regenerated cellulose (RC) following the method described by Liu.[26] The membrane was treated with a 0.5 M KOH solution (ethanol/deionized water = 1:1, v/v) and shaken for 3 hours at ambient temperature. It was then thoroughly washed with deionized water to remove any residual KOH from the nanofiber membrane. Then, the oxidation process was performed by treating the RC membrane with a $NaIO_4$ solution (4.2 mg/mL) prepared in glycine buffer solution (GBS, 0.05 M, pH 9.0). The membrane was shaken in this solution at 30 °C for 6.8 hours. After the oxidation process, the membrane was thoroughly rinsed with deionized water and designated as oxidized cellulose (OC).

The modification process began with glutaraldehyde activation. The oxidized cellulose (OC) membrane was soaked in a 2% glutaraldehyde solution at 25 °C for 2 hours to introduce aldehyde groups. The activated nanofiber membrane was then rinsed several times with glycine buffer solution (GBS, 0.05 M, pH 9.0) to remove any residual glutaraldehyde. Next, a spacer arm, nitrilotriacetic acid (NTA), was prepared and used to soak the nanofiber membrane. The final step of surface modification involved coupling NTA with nickel by immersing the membrane in a 0.5 M $NiCl_2$ solution and shaking at 37 °C and 150 rpm for 24 hours. Nickel strongly binds to the His-tag on recombinant lipase ITB 1.2, facilitating lipase immobilization.

2.3 Lipase immobilization onto OC nanofibers

A recombinant lipase solution (24 mg/mL) was prepared by dissolving an appropriate amount of lipase in glycine buffer solution (GBS, 0.05 M, pH 9.0). The oxidized cellulose (OC) nanofiber membrane was submerged in 20 mL of the lipase solution and incubated in a shaking water bath at 25 °C for 2 hours. Covalent coordination binding occurred between nickel and lipase. Following immobilization, the CNF-lipase complex was removed and gently washed three times with 10 mL of GBS (0.05 M, pH 9.0). The used washing buffer was collected, and the protein concentration was determined using the Bradford assay.[27] Enzyme loading is expressed as the amount of lipase (mg) per gram of fibers, calculated based on the difference in protein mass balance between the initial and

final lipase solution, including any remaining washings. A calibration curve was constructed using bovine serum albumin (BSA) as a standard. The immobilization yield determined in Eq. (1) C_1 and C_2 refer to initial and final protein concentration.

$$\text{Immobilization yield } (\%)=\frac{C_1-C_2}{C_1}\times 100 \quad (1)$$

2.4 Hydrolysis reaction

The performance of immobilized lipase was investigated using a Rotating Bed Reactor (RBR) under batch conditions. The RBR configuration allowing our previous study.[5] The hydrolysis reaction was conducted in the RBR with a two-phase substrate consisting of varied palm oil and water ratio. The reaction was carried out at 60 °C, pH 9.0 followed recombinant lipase ITB 1.2 optimum conditions.[16] It takes 9 hours reaction time in each cycle to obtain the optimum fatty acid yield as the main product, with bed rotational speed as the variable. The percentage of hydrolysis was described as number of fatty acids in the sample per maximum theoretical amount as calculated in Eq. (2)

$$\text{Hidrolisis } (\%)=\frac{V_{KOH}\times 10^{-3}\times M_{KOH}\times MM}{Wt\times f}\times 100 \quad (2)$$

where V is volume of potassium hydroxide solution required during titration, M is potassium hydroxide concentration, MM for fatty acid average molecular mass, Wt is weight of sample, and *f* is fraction of oil at initial reaction. The catalytic enzyme efficiency was present as Turnover Frequency (TOF) defined as the number of substrate molecules converted into product per unit time, normalized by the amount of lipase present expressed at Eq. (3)

$$\text{TOF}=\frac{r_a \text{ x volume}}{\text{moles of lipase}} \quad (3)$$

It is calculated as the reaction rate divided by the total amount of lipase. The reaction rate, r_a represents the rate of reaction at a given time, while the volume refers to the total volume of the reaction system.

2.5 Scanning Electron Microscopy (SEM) analysis

The morphology and diameter of the cellulose nanofibers were analysed by SEM. A 3500 SU SEM apparatus was operated at an excitation voltage of 10 kV with a magnification of 5000×. SEM images were processed and analysed using ImageJ software version 1.53, National Institutes of Health[28] to determine the fibers diameter distribution. The composition of cellulose nanofibers was analysed starting with surface coating of CNF with osmium, followed by scanning electron microscopy (SEM) (Model S2400, Hitachi, Japan) for morphological analysis, and energy-dispersive X-ray spectroscopy (EDX) for elemental composition determination.

2.6 X-ray Photoelectron Spectroscopy (XPS) analysis

The chemical composition during the modification steps was analysed using XPS. A Kratos Axis Ultra HAS XPS device was employed for chemical identification, utilizing a monochromatic Al source operated at 90 W. The quantification of nickel presence was conducted following the method described by Biesinger.[39] Four elements were identified: carbon, oxygen, nickel, and nitrogen.

2.7 Nitrogen physisorption analysis

The nanofibers pore structure and specific surface area were performed using nitrogen adsorption-desorption isotherm at liquid nitrogen boiling point temperature using by Tristar Kr 3020, USA Micromeritics device. The nanofibers were degassed at 50 °C under vacuum for 6 hours before examined. The Braunauer -Emmet-Teller (BET) multi point method identified the pore size distribution and specific surface area was conducted by Barrett- Joyner-Halenda (BJH) method.[30]

2.8 Atomic Force Microscopy (AFM) analysis

The topography of cellulose nanofibers was analysed using atomic force microscopy (AFM) with an AFM5400L instrument (Hitachi, Japan). AFM measurements provided the average surface roughness of the cellulose nanofiber samples by assessing probe interactions with the sample surface.

2.9 Fourier Transform Infrared (FTIR) analysis

The analysis of functional groups on cellulose nanofiber during the modification and immobilization process was characterized by FTIR. A PerkinElmer Frontier FTIR apparatus was utilized to obtain functional group information by analysing the spectral data in the infrared region (4000–400 cm^{-1}).

2.10 Lipase catalytic activity

In this study, specific activity and relative activity were used to evaluate the catalytic performance of the enzyme. Specific activity was defined as the amount of lipase activity per milligram of protein. Meanwhile, relative activity was expressed as the ratio of the specific activity of immobilized lipase to that of free lipase.[15] The enzymatic activity of both immobilized and free lipase was determined based on the amount of p-nitrophenol (p-NP) produced by a specific quantity of lipase over a given period. One enzyme unit was defined as the amount of biocatalyst required to liberate 1.0 µmol of p-NP per minute under the specified conditions.[31] The activity of immobilized lipase in an aqueous medium was assessed following the methods described by Chiou and Wu (2004) and Chen (2011).[10,32] The reaction was initiated by immersing 1.0 mg of immobilized lipase in a reaction mixture consisting of 1.0 mL of ethanol containing 14.4 mM p-nitrophenyl palmitate (p-NPP) and 1.0 mL of glycine buffer solution (GBS, 0.05 M, pH 9.0). The reaction mixture was then incubated at 60 °C. After 5 minutes, the reaction was terminated by adding 2.0 mL of 0.5 M Na_2CO_3, followed by centrifugation at 5,000 rpm for 15 minutes. A 0.5 mL aliquot

of the supernatant was diluted in Milli-Q water and analysed using a UV-Vis spectrophotometer (UV-2450, Shimadzu, Japan) at 420 nm. The blank sample consisted of GBS (0.05 M, pH 9.0), while the control solution contained the complete reaction mixture without lipase.

3. Results and discussion

3.1 Synthesis

3.1.1 Synthesis cellulose acetate (CA) nanofibers

In addition to molecular weight, solvent type, humidity, and the spinning ability of the solution, fiber formation is also significantly influenced by solution concentration and electrical conductivity. In fiber production, a minimum concentration is required to achieve chain entanglement which is important for the transition from electrospraying to electrospinning.[33] If the concentration is too high, overcoming the viscoelastic force becomes challenging, preventing jet formation. Conversely, reducing the concentration favors the formation of thinner fibers. In general, a decrease in viscosity and surface tension facilitates the production of finer fibers.[34] The morphology of cellulose acetate nanofibers at various concentrations was analyzed using SEM SU3500, as shown in Fig. 1. At a 15% CA concentration (Fig. 1 (b)), fibers with a diameter of 660 nm were produced (Fig. 1(d)), whereas a 25% CA concentration (Fig. 1 (c)), resulted in larger fibers with a diameter of 880 nm (Fig. 1 (e)), Considering surface area optimization, the 15% CA concentration was selected for further research.

3.1.2 Oxidized cellulose nanofibers (OC)

The oxidation of regenerated cellulose (RC) using $NaIO_4$ successfully introduced aldehyde functional groups, producing oxidized cellulose (OC). As observed in Fig. 2, the transition from CA to RC membranes resulted in noticeable shrinkage due to deacetylation, while the OC membrane exhibited further shrinkage and increased surface roughness after oxidation. This shrinkage was evident from the reduced spacing between fibers in both RC and OC nanofiber. However, despite these modifications, the fiber structure and diameter remained intact, demonstrating the robustness of the nanofiber framework. These findings confirm the feasibility of using modified CA nanofiber membranes for hydrolysis reactions, as the structural integrity necessary for enzymatic applications was maintained.

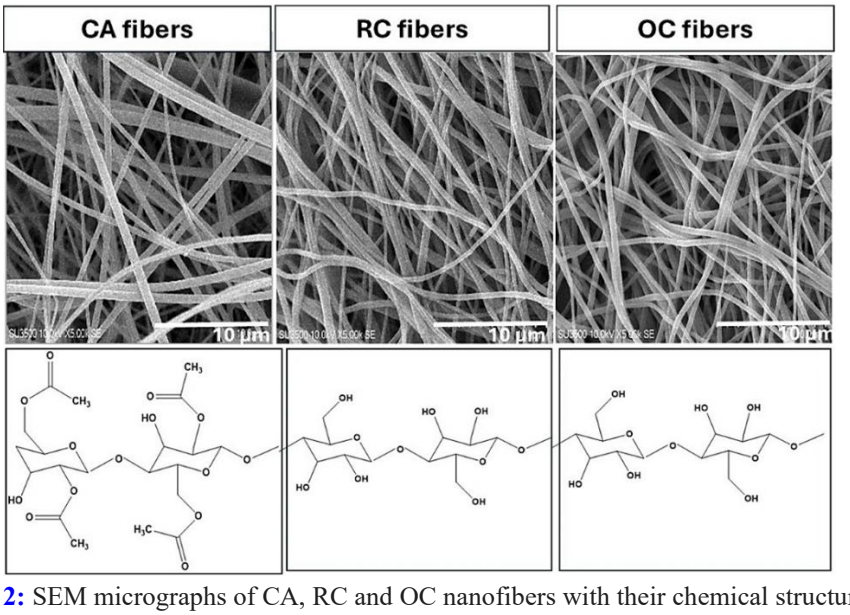

Fig. 2: SEM micrographs of CA, RC and OC nanofibers with their chemical structures.

3.2 Mechanism of CNF surface modification and immobilization

The surface modification process of CNF involves a series of chemical bonding. Initially, glutaraldehyde facilitates the bonding between aldehyde groups on the oxidized cellulose (OC) and amino groups, forming a stable imine (N=C) bond while releasing water. Subsequently, nitrilotriacetic acid (NTA) is attached through amine ($-NH_2$) interactions, forming an APTES-Glu-NTA linkage.

In the next step, Ni^{2+} from $NiCl_2$ coordinates with the NTA complex via its three carboxyl groups and nitrogen atoms, establishing a stable metal-ligand complex. The Ni^{2+} ion, which has six coordination sites, stabilizes with two H_2O molecules, while the remaining sites remain available for enzyme immobilization Fig. 3. Upon immersing the modified CNF into the $NiCl_2$ solution, an ionization reaction occurs where Ni^{2+} interacts with H_2O, forming nickel hydroxide ($NiOH_2$) as described in Eq. (4) and (5). The OH^- ions are then displaced by lipase, which covalently coordination binds to the Ni^{2+} ion, completing the immobilization process. This mechanism ensures a stable and efficient enzyme attachment, enhancing catalytic performance.

$$NiCl_2 \rightarrow Ni^{2+} + Cl^- \quad (4)$$

$$Ni^{2+} + 2H_2O \rightarrow Ni(OH)_2 + 2OH^- \quad (5)$$

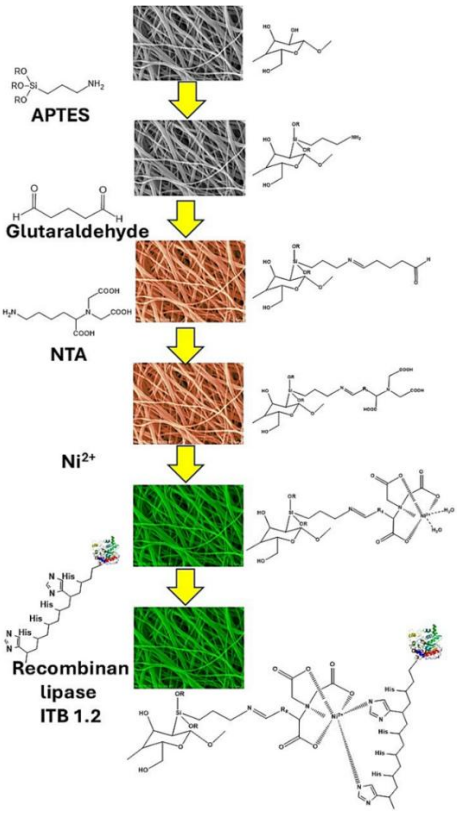

Fig. 3: Mechanism of surface modification and recombinant lipase ITB 1.2 immobilization into CNF.

Table 1: Immobilization of recombinant lipase ITB 1.2 on electro spun CNF with different fibres diameters and specific surface area.

Fiber diameters (nm)	Specific surface area (m^2/g)	Lipase loading (mg/g)	Yield Immobilization (%)	Specific Activity (U/mg)
660 ± 8.4	2.46	21.53	90.4	94.41
800 ± 17.3	1.32	18.30	88.0	107.61
Free lipase	-	-		133.28

The immobilization of recombinant lipase ITB 1.2 onto the CNF matrix is facilitated by the coordination between Ni^{2+} and the imidazole rings of histidine residues. This process involves the displacement of H_2O molecules from two of the six coordination sites of Ni^{2+}, allowing direct binding to two histidine residues on the enzyme. The imidazole ring of histidine contains a nitrogen atom with a lone electron pair, which forms a strong covalent coordination bond with Ni^{2+} as shown at Fig. 3.

The interaction between the His-tagged recombinant ITB 1.2 and the synthesized CNF nanofibers occurs primarily through physical adsorption, driven by Lewis base interactions, where the imidazole group of histidine donates electrons to metal ions.[35] The presence of His-tags at the N- or C-terminal facilitates seamless integration into target proteins through the addition of several amino acids. The interaction between nickel and the imidazole group of histidine enables reversible, oriented immobilization onto the solid surface of the matrix.[36–38]

3.3 Lipase immobilization into CNF under various fibres diameter

The fiber diameter was varied of 600 and 800 nm, and the corresponding enzyme loading and activity were analyzed in this study. The CNF matrix is expected to facilitate high enzyme loading due to its structural properties. Although CNF has a relatively low specific surface area, its large matrix volume compensates by providing ample space for enzyme immobilization. Table 1 presents the enzyme loading on CNF, examining the effect of fiber diameter on recombinant lipase immobilization. The results indicate that enzyme loading decreases as fiber diameter increases. Specifically, an enzyme loading of 18.3 mg/g was observed for fibers with an 800 nm diameter, whereas fibers with a 660 nm diameter exhibited a higher enzyme loading of 21.53 mg/g. The enhanced enzyme loading in smaller-diameter fibers is attributed to their larger surface area, which provides increased exposure of functional groups and a greater number of available binding sites for lipase immobilization. A large specific surface area must also be complemented by sufficient fiber strength to ensure endurance and mechanical stability during the reaction process. Both fiber diameters examined in this study were found to be suitable within the given range. However, for subsequent research, the 600 nm CNF nanofiber was selected due to its

surface area with a specific surface area of 2.46 m^2/g.

3.4 Characterisation

3.4.1 Atomic force microscopy (AMF)

The topographical differences of CNF before and after immobilization were clearly observed using atomic force microscopy, as shown in Fig. 4. The images reveal that the CNF surface before immobilization was smooth and uniform (Fig. 4 (a)) . In contrast, after immobilization, the CNF exhibited a rough, wrinkled, and folded surface, indicating successful modification and lipase attachment (Fig. 4 (b)). This phenomenon occurred due to the addition of chemical functional materials and spacer arms during the modification and immobilization process, which introduced specific functional groups and allowed the lipase to penetrate deeply into the CNF matrix. Moreover, the difference in surface roughness before and after immobilization was significant. The CNF exhibited average surface roughness of 1017 nm before immobilization, which increased slightly to 6068 nm after immobilization.

3.4.2 N_2 physisorption

The synthesized CNF (OC membrane) was characterized using nitrogen adsorption-desorption analysis, revealing a type IV isotherm, indicative of a porous material. As shown in Fig 6, the adsorption isotherm curve Fig. 4 (c) exhibits an H1 hysteresis loop, while the BJH pore radius distribution Fig. 4 (d) indicates a predominant pore size of 5.5 nm. These results confirm that the CNF membrane falls within the mesoporous category, with a minor fraction of micropores measuring approximately 2 nm in radius. The specific surface area, calculated using the Brunauer-Emmett-Teller (BET) method[39] as determined to be 2.46 m^2/g.

3.4.3 Fourier transform infrared (FTIR)

Cellulose nanofibers were further characterized using FTIR/ATR spectroscopy, as shown in Fig. 4 (e). The CNF spectra exhibited three distinct peaks at 1230 cm^{-1} (C–O–C), 1375 cm^{-1} ($C–CH_3$), and 1745 cm^{-1} (C=O), which correspond to the oscillation of acetate groups. These peaks disappeared following the deacetylation process, confirming the successful removal of acetyl groups from the CNF surface. Additionally, new peaks emerged after surface modification, including a strong peak at 1050 cm^{-1} (C–O), indicating the presence of oxidized cellulose (OC) nanofibers. The significant appearance of peaks at 1630 cm^{-1} (C–N) and 3400 cm^{-1} (N–H) in the immobilized CNF spectra closely matched those of lipase ITB 1.2, confirming the successful immobilization of lipase ITB 1.2 onto the CNF matrix.

3.4.4 X-Ray photoelectron spectroscopy (XPS)

Chemical modifications and immobilization on the CNF surface during the immobilization process were analyzed using X-ray photoelectron spectroscopy (XPS). Prior to modification, two primary elements were detected: carbon (C) and oxygen (O). Following the modification process, two additional elements, nitrogen (N) and nickel (Ni), emerged, as shown in Fig. 5 (a). The unmodified CNF exhibited two characteristic peaks: one at 285 eV, corresponding to C 1s, and another at 531.01 eV, attributed to O 1s, which represents the Ni–O–C bonding structure[40] or N-Ni-O[41] resulting from O coordination directly via the carbonyl group of Hiss tags. These two characteristic peaks underwent significant changes during the modification and immobilization process, indicating alterations in the chemical environment of the CNF surface (Fig. 5 (b) and (c)). The alkaline hydrolysis process for cellulose regeneration and subsequent oxidation using $NaIO_4$ resulted in an increase in the C and O elemental composition. The oxidation of oxygen atoms during surface modification elevated the oxidation state, leading to an increase in bond

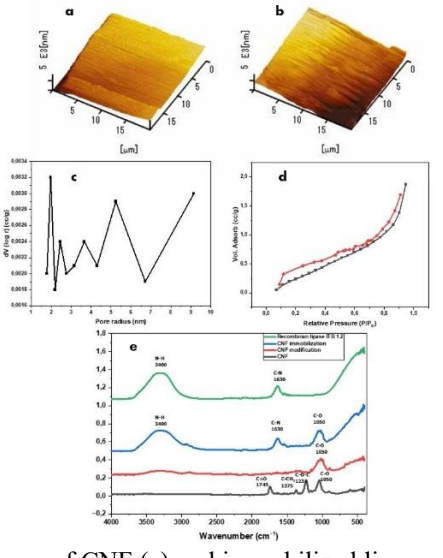

Fig. 4: Atomic force microscopy surface images of CNF (a) and immobilized lipase onto CNF (b). BET surface area and BJH pore diameter of CNF (c) adsorption-desorption relative pressure curve (d) pore radius. FTIR/ATR spectra of CNF, CNF modification, CNF immobilization and lipase ITB 1.2 (e).

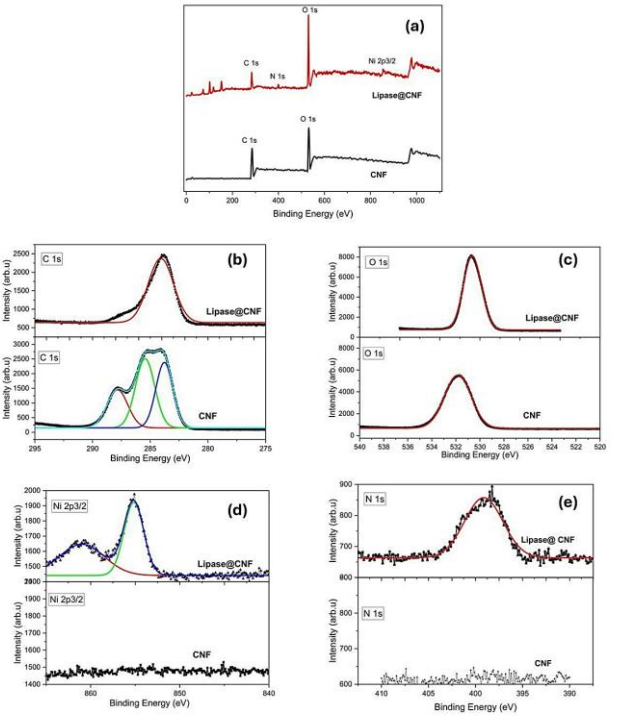

Fig. 5: X-ray photoelectron spectroscopy spectra (XPS) CNF (a), element C 1s (b), element O 1s (c), element Ni 2p (d) and element N 1s (e).

Table 2: CNF chemical composition during modification and immobilization process.

	C_{1s} (%)	O_{1s} (%)	N_{1s} (%)	Ni_{2p} (%)
CNF	73.55	26.44	-	-
CNF- Glu	70.54	29.46	-	-
CNF- Glu-NTA	45.43	44.73	7.48	-
CNF- Glu-NTA-Ni	43.49	42.17	7.21	8.13
CNF- Glu-NTA-Ni-Lip	44.71	33.98	13.67	7.64

energy and a corresponding peak shift toward higher energy levels (Fig. 5 (c)). An additional peak at 401 eV corresponds to the N 1s binding energy, detected on the fiber surface after the introduction of APTES and activators such as glutaraldehyde and NTA during the modification process (Fig. 5 (d)). Furthermore, the Ni element was identified at peaks 856.2 and 860.9 eV, which can be attributed to the Ni^{2+} $2p_3/_2$ orbital spin (Fig. 5 (e)). The presence of both N and Ni peaks confirms the successful modification process.

Table 2 presents the chemical composition in percentage. The addition of glutaraldehyde did not significantly alter the composition of carbon (C) and oxygen (O) during the modification process. The increase in oxygen (O) content after immobilization was attributed to the presence of acetyl groups resulting from NTA, while the rise in nitrogen (N) composition, particularly from 7.21% to 13.67%, confirmed the successful immobilization of ITB 1.2 lipase onto the CNF.

3.4.5 Scanning electron microscopy- energy dispersive X-ray (SEM EDX)

The morphology of cellulose nanofibers (CNF) primarily consists of carbon and oxygen (Fig. 6 (a)). Following the regeneration and oxidation processes, oxygen was more prominently distributed across the CNF surface (Fig. 6 (b) and (c)). After the immobilization process, the CNF morphology became more complex due to the chelation of various materials and lipase onto the fiber surfaces (Fig. 6(d)). The fiber structure compacted because of the modification steps, which potentially increased the surface area, facilitated unrestricted lipase attachment, and enhanced overall process efficiency. The addition of spacer arms and nickel ions during the modification process contributed to a denser fiber network. Elemental analysis by EDX mapping (Fig. 6(e)) revealed the presence of carbon (33.2%), oxygen (44.5%), nickel (19.2%), and nitrogen (3.1%), uniformly distributed across the CNF surface. The presence of nitrogen further confirmed the successful immobilization of lipase onto the cellulose nano fibers. Table 3 summarizes the comparison of lipase immobilization in nanofiber matrices over the years. Specifically, in the CNF matrix, this study demonstrates superior performance in both enzyme loading and relative activity. Compared to bulk materials, CNF exhibits enhanced enzymatic activity by improving mass transport of substrate molecules to and from the active site.[42]

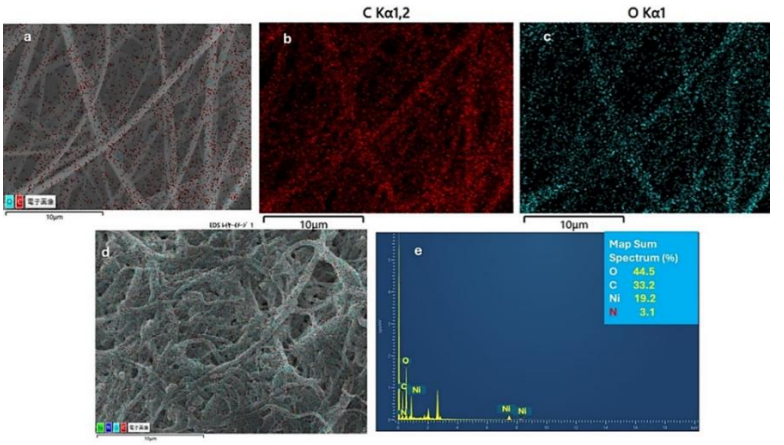

Fig. 6: Morphology of cellulose nanofiber CNF before treatment (a); distribution of C (b); O (c) on CNF; immobilized lipase onto CNF (d); distribution element of N, Ni, O, C (e) (f).

Table 3: Current research of enzyme immobilization into nanofiber.

Matrix	Protein loading (mg/g fibers)	Relative activity (%)	Reusability	Ref.
Cellulose Nanofiber (CNF)	21.53	70.8 (60°C)	3 (9 h)	This Study
Cellulose Acetate Nanofiber (CNF)-poly (ethylene terephthalate)	-	43 (60°C)	13 (1.5 h)	[47]
Cellulose Nanofiber (CNF)	-	80 (50°C)	6 (3h)	[48]
Bacterial Cellulose Nanofiber	-	69.6	9 (-)	[49]
Polyethylene oxide /alginate nanofibers	-	65–70	14 (0.25 h)	[50]
Cellulose Nanofiber (CNF)	-	29.6	2 (6.8 h)	[15]
Cellulose Nanofiber (CNF)	28.9	44.3	-	[16]
Polyacrylonitrile nanofibers	15-25	75	7 (-)	[51]
Polycaprolactone nanofibers	3–5	-	10 (0.5 h)	[52]
Poly (acrylonitrile-co-maleic acid)	21.3	37.6	-	[53]
Poly acrylonitrile	21.2	81.3	10 (1 h)	[54]
Nanofiber polystyrene/poly (styrene-*co*-maleic anhydride) composite	5.6	16.5	-	[55]
Nanofibrous Poly (acrylonitrile-co- maleic acid)	20.7	49.7	10(2 h)	[56]

3.4.6 Catalytic properties of immobilized recombinant lipase ITB 1.2

The catalytic performance of immobilized lipase on CNF was evaluated under varying pH and temperature conditions, as illustrated in Fig 7. The effect of pH on enzyme activity is shown in Fig. 7(a). The activity of the immobilized lipase reached its maximum at pH 9.5, whereas the optimum pH for the free enzyme was observed at pH 9.0.[22] This shift in optimum pH is likely attributed to changes in the microenvironment surrounding the immobilized enzyme, possibly due to electrostatic interactions between the lipase and the CNF-based support material.[43] A comparable observation was reported by Katrolia *et al.*, where immobilization of commercial galactosidase onto chitosan and alginate resulted in a reduction in enzyme activity at elevated pH values for both the free and immobilized forms.[44] Although the optimum pH was identified at 9.5, the experiments were conducted at pH 9 to maintain consistency with previous studies[5] This approach ensures data comparability and facilitates a more reliable interpretation of the results. Moreover, although the optimum pH of the immobilized enzyme is 9.5, its activity at pH 9 remains relatively high and falls within the optimal pH range.

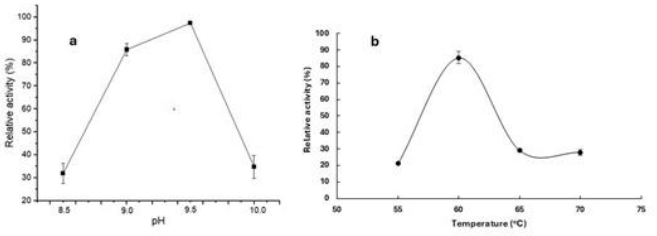

Fig. 7: Effect of (a) pH, (b) temperature on lipase immobilized-CNF activity.

The effect of temperature on catalytic activity is depicted in Fig. 7(b). Both the free and immobilized lipase exhibited maximum activity at 60 °C, suggesting that the immobilization process did not alter the enzyme's optimal temperature. This finding aligns with results reported by Andrade, who demonstrated that both recombinant galactosidase and its chitosan-immobilized form exhibited identical optimal temperatures at 50 °C.[23] However, at temperatures above 60 °C, a significant loss of activity was observed for the immobilized lipase.

3.5 Hydrolysis reaction

The hydrolysis reaction was carried out in a rotating bed reactor (RBR) with immobilized CNF contained within a basket, allowing reactor configuration our previous research.[5] In lipase-catalysed hydrolysis, water acts as a key substrate because lipase binds to triglycerides at the oil–water interface, where the reaction takes place. The influence of substrate concentration on hydrolysis efficiency is illustrated in Fig. 8(a). Among the tested conditions, an oil-to-water ratio of 1:9 (v/v) was identified as the optimal substrate mixture, resulting in the highest hydrolysis efficiency. Although the 1:6 ratio produced a comparable yield, the 1:9 ratio achieved superior results with a lower amount of substrate, thereby establishing it as the optimum ratio When the oil-to-water ratio deviates beyond a certain optimal range either by increasing or decreasing., the hydrolysis reaction becomes less efficient, leading to a reduction below 63%. At low water-oil ratio, the hydrolysis reaction tends to shift toward the reverse reaction. Moreover, insufficient water content may lead to increased viscosity in the reaction mixture, potentially resulting in mass transfer limitations that hinder effective interactions between the substrate and lipase.[45] Conversely, an excessively high water-oil ratio may cause leaching of lipase from the solid support, thereby reducing catalytic activity and overall conversion.[46] These findings underscore the critical importance of maintaining an appropriate oil-to-water ratio in the reaction mixture to ensure both optimal enzymatic activity and high conversion in this research.

The rotational speed of the reactor basket was adjusted to evaluate its effect on mass transfer efficiency. At rotational speeds of 600 and 500 rpm, the hydrolysis yield reached 63% and 57%, respectively, over 8 hours. In contrast, at 400 rpm, the hydrolysis yield was significantly lower, reaching only 40 % within the same reaction time (Fig. 8(b)). The higher

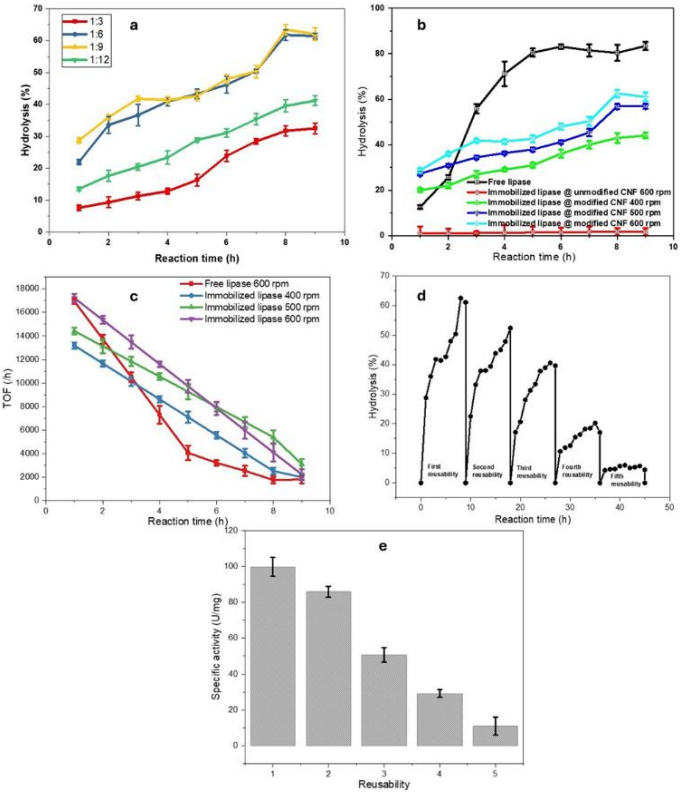

Fig. 8: Effect of substrate concentration, ratio oil/water (v/v) on hydrolysis conversion (a). Effect of rotation speed on % hydrolysis conversion in RBR reactor (b) Turn over frequency lipase ITB 1.2(c), reusability CNF matrix in RBR (d) and specific activity during reusability (e).

rotational speeds in the RBR facilitated increased collisions between the substrate and the CNF support within the rotor packing, thereby enhancing mixing between the oil and water phases, increasing the contact area, and improving mass transfer between the two phases. In contrast, free enzyme obtained almost 83% hydrolysis yield conversion which contained higher enzyme loading (24 mg/g) than that of immobilized enzyme (21.53 mg/g). Acting as a control, lipase immobilized on unmodified CNF at a rotational speed of 600 rpm yielded merely ~1% hydrolysis (represented by the red line). This clearly demonstrates the substantial enhancement in enzymatic efficiency achieved through CNF modification.

From the perspective of Turnover Frequency (TOF), which refers to the number of substrate molecules converted into product per lipase molecule over a given time, the immobilized enzyme exhibited superior performance compared to the free enzyme (Fig. 8(c)). This indicates that immobilized lipase is a more effective approach for achieving higher conversion rates. Additionally, the reusability of the immobilized enzyme in the RBR was assessed. Five reaction cycles were performed at 600 rpm over a total duration of 45 hours. In the first cycle, the conversion slightly increased to 63%, and the enzyme maintained its activity over three successive cycles. However, in the fourth and fifth cycles, the conversion rate declined significantly, reducing to nearly half of the initial conversion (Fig. 8(d)).

A gradual decrease in immobilized lipase activity was observed during repeated exposure in the rotational system. Mechanical forces likely contributed to this decline in activity over multiple cycles. Additionally, factors such as enzyme leaching, desorption, and other potential mechanisms may have played a role. Fig. 8(e) illustrates the reduction in specific activity with repeated use, confirming that enzyme leakage was a primary reason for the declining hydrolysis conversion. The loss of specific activity was further supported by measuring the lipase activity in the supernatant after each cycle. Beyond the fifth cycle, enzyme activity became negligible and was no longer detectable. Despite this decline, the immobilized lipase demonstrated significant reusability, retaining more than 50% of its initial activity after three cycles. This makes it a viable option for applications requiring high enzyme reusability.

4. Conclusion

Recombinant lipase ITB 1.2 was successfully immobilized onto a CNF matrix through surface modification and the incorporation of an NTA/Ni spacer arm. The immobilized lipase demonstrated reusability in hydrolysis reactions for fatty acid production. The combination of a modified CNF surface with a spacer arm effectively maintained lipase conformation while enhancing substrate accessibility, as evidenced by the high hydrolysis conversion achieved. The CNF surface modification and Ni-bound spacer arm facilitated covalent coordination with the His-tagged recombinant lipase ITB 1.2. This method will also be applied to other enzymes in subsequent studies. Further optimization of each modification step is necessary to improve the cost-effectiveness of this process. Future research should prioritize the integration of process intensification and cost-effectiveness, with particular emphasis on improving high throughput using microbioreactor as a key area of investigation. Continuous process mode may also be implemented with new reactor configuration.

Acknowledgments

The authors sincerely thank BPDP Kelapa Sawit Indonesia for their financial support under contract number PRJ-65/DPKS/2023. The authors also extend their appreciation to Gifu University for granting laboratory access for material characterization in this research. Additionally, the authors would like to thank Makoto Torazawa, Ryo Hashimoto, and Tatsuya Suzuki for their valuable assistance in the laboratory.

Conflict of Interest

The authors disclose that this research was funded by BPDP Kelapa Sawit Indonesia. However, the funding body had no role in study design, data collection, analysis, interpretation, or manuscript preparation.

Supporting Information

Not applicable.

Ethical Statement

This article does not contain any studies with human participant or animals performed by any authors.

CRediT Statement

Ghusrina Prihandini: Writing – Original draft, Methodology, Investigation, Formal analysis, Data curation. **Wilda Panjaitan:** Investigation, Data curation. **Elvi Restiawaty:** Writing – Review & editing, Methodology, Investigation, Funding acquisition, Formal analysis, Conceptualization. **Dian Ahmad Hapidin:** Methodology, Formal analysis. **Akhmaloka Akhmaloka:** Supervision, Methodology, Formal analysis, Investigation, Conceptualization. **Yogi Wibisono Budhi:** Writing – Review & editing, Supervisions, Methodology, Investigation, Funding acsquisition, Formal analysis, Conceptualization.

References

[1] C. Silva Almeida, F. Simão Neto, P. da Silva Sousa, F. I. da Silva Aires, J. R. de Matos Filho, A. L. Gama Cavalcante, P. G. de Sousa Jr, R. L. F. Melo, J. C. S. dos Santos, Enhancing lipase immobilization *via* physical adsorption: advancements in stability, reusability, and industrial applications for sustainable biotechnological processes, *ACS Omega*, 2024, **9**, 46698-46732, doi: 10.1021/acsomega.4c07088.

[2] R. C. Rodrigues, J. J. Virgen-Ortíz, J. C. S. dos Santos, Á. Berenguer-Murcia, A. R. Alcantara, O. Barbosa, C. Ortiz, R.

Fernandez-Lafuente, Immobilization of lipases on hydrophobic supports: immobilization mechanism, advantages, problems, and solutions, *Biotechnology Advances*, 2019, **37**, 746-770, doi: 10.1016/j.biotechadv.2019.04.003.

[3] E. Restiawaty, F. Arabica Yatasya, Ellys, N. Tresna Umi Culsum, Akhmaloka, Y. Wibisono Budhi, Lipase immobilization onto Cellulose Nanocrystals (CNC) for catalyzing lipolysis of triglycerides, *IOP Conference Series: Materials Science and Engineering*, 2021, **1143**, 012009, doi: 10.1088/1757-899x/1143/1/012009.

[4] N. T. U. Culsum, A. Wibowo, Subagjo, Y. W. Budhi, Fabrication of lipase immobilized-carboxylated cellulose nanocrystals as biocatalyst for enzymatic hydrolysis of palm oil and its kinetical study, *Biocatalysis and Agricultural Biotechnology*, 2023, **54**, 102915, doi: 10.1016/j.bcab.2023.102915.

[5] W. Panjaitan, G. Prihandini, E. Restiawaty, H. P. Rendra Graha, M. Miyamoto, S. Uemiya, A. Akhmaloka, Y. W. Budhi, Enhanced fatty acid production using recombinant Lipase in a Rotating Bed Reactor (RBR), *Case Studies in Chemical and Environmental Engineering*, 2024, **10**, 101017, doi: 10.1016/j.cscee.2024.101017.

[6] H. Bai, D. Yu, X. Du, Review of porous microspheres for enzyme immobilization: Strategies, applications, and prospects, *International Journal of Biological Macromolecules*, 2025, **295**, 139627, doi: 10.1016/j.ijbiomac.2025.139627.

[7] L. Bayne, R. V. Ulijn, P. J. Halling, Effect of pore size on the performance of immobilised enzymes, *Chemical Society Reviews*, 2013, **42**, 9000, doi: 10.1039/c3cs60270b.

[8] Z. Li, D. Pan, Z. Han, D. J. P. Kumar, J. Ren, H. Hou, Z. M. El-Bahy, G. A. M. Mersal, B. B. Xu, Y. Liu, C. Liu, M. M. Ibrahim, Boron nitride whiskers and nano alumina synergistically enhancing the vertical thermal conductivity of epoxy-cellulose aerogel nanocomposites, *Advanced Composites and Hybrid Materials*, 2023, **6**, 224, doi: 10.1007/s42114-023-00804-3.

[9] H. Liu, Y.-L. Hsieh, Ultrafine fibrous cellulose membranes from electrospinning of cellulose acetate, *Journal of Polymer Science Part B: Polymer Physics*, 2002, **40**, 2119-2129, doi: 10.1002/polb.10261.

[10] P.-C. Chen, X.-J. Huang, F. Huang, Y. Ou, M.-R. Chen, Z.-K. Xu, Immobilization of lipase onto cellulose ultrafine fiber membrane for oil hydrolysis in high performance bioreactor, *Cellulose*, 2011, **18**, 1563-1571, doi: 10.1007/s10570-011-9593-0.

[11] S. Ahmed, R. A. Khan, T. U. Rashid, Cellulose nanocrystal based electrospun nanofiber for biomedical applications–a review, *Carbohydrate Polymers*, 2025, **348**, 122838, doi: 10.1016/j.carbpol.2024.122838.

[12] W. Huang, Y. Zhan, X. Shi, J. Chen, H. Deng, Y. Du, Controllable immobilization of naringinase on electrospun cellulose acetate nanofibers and their application to juice debittering, *International Journal of Biological Macromolecules*, 2017, **98**, 630-636, doi: 10.1016/j.ijbiomac.2017.02.018.

[13] A. Khodayari, S. Vats, G. Mertz, C. N. Schnell, C. F. Rojas, D. Seveno, Electrospinning of cellulose nanocrystals; procedure and optimization, *Carbohydrate Polymers*, 2025, **347**, 122698, doi: 10.1016/j.carbpol.2024.122698.

[14] D. Thi My Huong, C.-Y. Wang, P.-Y. Chen, C. W. Ooi, X. E. C. Thew, B.-L. Liu, C.-Y. Chiu, S.-L. Tsai, K.-H. Chen, Y.-K. Chang, Immobilization of poly(hexamethylene biguanide) to cellulose acetate- and cellulose-based nanofiber membranes for antibacterial and cytotoxic studies, *Biochemical Engineering Journal*, 2024, **205**, 109256, doi: 10.1016/j.bej.2024.109256.

[15] X.-J. Huang, P.-C. Chen, F. Huang, Y. Ou, M.-R. Chen, Z.-K. Xu, Immobilization of Candida rugosa lipase on electrospun cellulose nanofiber membrane, *Journal of Molecular Catalysis B: Enzymatic*, 2011, **70**, 95-100, doi: 10.1016/j.molcatb.2011.02.010.

[16] P.-C. Chen, X.-J. Huang, Z.-K. Xu, Utilization of a biphasic oil/aqueous cellulose nanofiber membrane bioreactor with immobilized lipase for continuous hydrolysis of olive oil, *Cellulose*, 2014, **21**, 407-416, doi: 10.1007/s10570-013-0148-4.

[17] A. Badoei-dalfard, A. Tahami, Z. Karami, Lipase immobilization on glutaraldehyde activated graphene oxide/chitosan/cellulose acetate electrospun nanofibrous membranes and its application on the synthesis of benzyl acetate, *Colloids and Surfaces B: Biointerfaces*, 2022, **209**, 112151, doi: 10.1016/j.colsurfb.2021.112151.

[18] G. Kuang, Z. Wang, X. Luo, Z. Geng, J. Cui, M. Bilal, Z. Wang, S. Jia, Immobilization of lipase on hydrophobic MOF synthesized simultaneously with oleic acid and application in hydrolysis of natural oils for improving unsaturated fatty acid production, *International Journal of Biological Macromolecules*, 2023, **242**, 124807, doi: 10.1016/j.ijbiomac.2023.124807.

[19] M. Oshige, K. Yumoto, H. Miyata, S. Takahashi, M. Nakada, K. Ito, M. Tamegai, H. Kawaura, S. Katsura, Immobilization of his-tagged proteins on various solid surfaces using NTA-modified chitosan, *Open Journal of Polymer Chemistry*, 2013, **3**, 6-10, doi: 10.4236/ojpchem.2013.31002.

[20] J. H. Forstater, S. T. Grosser, Data-rich process development of immobilized biocatalysts in flow, *Reaction Chemistry & Engineering*, 2022, **7**, 866-876, doi: 10.1039/d1re00298h.

[21] R. Yang, N. Zheng, Z. Yu, F. Zhang, H. Gai, J. Chen, X. Huang, Nickel foam/Covalent-Organic Frameworks for composite phase change materials with enhanced solar-thermal energy conversion and storage capacity, *Applied Thermal Engineering*, 2023, **230**, 120808, doi: 10.1016/j.applthermaleng.2023.120808.

[22] A. H. Permana, F. M. Warganegara, D. Wahyuningrum, M. P. Widhiastuty, A. Akhmaloka, Heterologous expression and characterization of thermostable lipases from geobacillus thermoleovorans PPD2 through escherichia coli, *Biosciences, Biotechnology Research Asia*, 2017, **14**, 1081-1088, doi: 10.13005/bbra/2545.

[23] B. C. de Andrade, A. Gennari, G. Renard, E. V. Benvenutti, J. M. Chies, G. Volpato, C. F. Volken de Souza, Nickel-functionalized chitosan for the oriented immobilization of histidine-tagged enzymes: a promising support for food bioprocess applications, *Catalysis Letters*, 2022, **152**, 2956-2970, doi: 10.1007/s10562-021-03912-1.

[24] N. M. Deraz, The comparative jurisprudence of catalysts preparation methods: II. Deposition-precipitation and adsorption methods., *Journal of Industrial Environmental Chemistry*, 2014, **2**, 1–5, http://www.alliedacademies.org/journal-industrial-environmental-chemistry/.
[25] D. Kowalczykiewicz, K. Szymańska, D. Gillner, A. B. Jarzębski, Rotating bed reactor packed with heterofunctional structured silica-supported lipase. Developing an effective system for the organic solvent and aqueous phase reactions, *Microporous and Mesoporous Materials*, 2021, **312**, 110789, doi: 10.1016/j.micromeso.2020.110789.
[26] H. Liu, Y.-L. Hsieh, Ultrafine fibrous cellulose membranes from electrospinning of cellulose acetate, *Journal of Polymer Science Part B: Polymer Physics*, 2002, **40**, 2119-2129, doi: 10.1002/polb.10261.
[27] M. Bradford, A rapid and sensitive method for the quantitation of microgram quantities of protein utilizing the principle of protein-dye binding, *Analytical Biochemistry*, 1976, **72**, 248-254, doi: 10.1006/abio.1976.9999.
[28] T. J. Collins, ImageJ for microscopy, *BioTechniques*, 2007, **43**, S25-S30, doi: 10.2144/000112517.
[29] M. C. Biesinger, B. P. Payne, L. W. M. Lau, A. Gerson, R. S. C. Smart, X-ray photoelectron spectroscopic chemical state quantification of mixed nickel metal, oxide and hydroxide systems, *Surface and Interface Analysis*, 2009, **41**, 324-332, doi: 10.1002/sia.3026.
[30] S. Grimme, J. Antony, S. Ehrlich, H. Krieg, A consistent and accurate *ab initio* parametrization of density functional dispersion correction (DFT-D) for the 94 elements H-Pu, *The Journal of Chemical Physics*, 2010, **132**, 154104, doi: 10.1063/1.3382344.
[31] Z. O. Malaibari, Effect of MWCNTs surface properties on lipase immobilization and its catalytic activity, *Materials Express*, 2018, **8**, 123-132, doi: 10.1166/mex.2018.1414.
[32] S.-H. Chiou, W.-T. Wu, Immobilization of Candida rugosa lipase on chitosan with activation of the hydroxyl groups, *Biomaterials*, 2004, **25**, 197-204, doi: 10.1016/s0142-9612(03)00482-4.
[33] O. Husain, W. Lau, M. Edirisinghe, M. Parhizkar, Investigating the particle to fibre transition threshold during electrohydrodynamic atomization of a polymer solution, *Materials Science and Engineering: C*, 2016, **65**, 240-250, doi: 10.1016/j.msec.2016.03.076.
[34] S. Talwar, A. S. Krishnan, J. P. Hinestroza, B. Pourdeyhimi, S. A. Khan, Electrospun nanofibers with associative polymer–surfactant systems, *Macromolecules*, 2010, **43**, 7650-7656, doi: 10.1021/ma1013447.
[35] E. K. M. Ueda, P. W. Gout, L. Morganti, Current and prospective applications of metal ion–protein binding, *Journal of Chromatography A*, 2003, **988**, 1-23, doi: 10.1016/s0021-9673(02)02057-5.
[36] G. Cao, J. Gao, L. Zhou, Z. Huang, Y. He, M. Zhu, Y. Jiang, Fabrication of Ni_2 +-nitrilotriacetic acid functionalized magnetic mesoporous silica nanoflowers for one pot purification and immobilization of His-tagged ω-transaminase, *Biochemical Engineering Journal*, 2017, **128**, 116-125, doi: 10.1016/j.bej.2017.09.019.
[37] S. Xue, J. Li, L. Zhou, J. Gao, G. Liu, L. Ma, Y. He, Y. Jiang, Simple purification and immobilization of his-tagged organophosphohydrolase from cell culture supernatant by metal organic frameworks for degradation of organophosphorus pesticides, *Journal of Agricultural and Food Chemistry*, 2019, **67**, 13518-13525, doi: 10.1021/acs.jafc.9b05206.
[38] Y. Li, P. Luan, L. Zhou, S. Xue, Y. Liu, Y. Liu, Y. Jiang, J. Gao, Purification and immobilization of His-tagged organophosphohydrolase on yolk–shell Co/C@SiO_2@Ni/C nanoparticles for cascade degradation and detection of organophosphates, *Biochemical Engineering Journal*, 2021, **167**, 107895, doi: 10.1016/j.bej.2020.107895.
[39] S. Brunauer, P. H. Emmett, E. Teller, Adsorption of gases in multimolecular layers, *Journal of the American Chemical Society*, 1938, **60**, 309-319, doi: 10.1021/ja01269a023.
[40] H. R. Harald Hantsche, *Advance Materials*, 1993, **5**, 778–1010.
[41] J. Huang, Y. Sun, X. Du, Y. Zhang, C. Wu, C. Yan, Y. Yan, G. Zou, W. Wu, R. Lu, Y. Li, J. Xiong, Cytomembrane-structure-inspired active Ni–N–O interface for enhanced oxygen evolution reaction, *Advanced Materials*, 2018, **30**, 1803367, doi: 10.1002/adma.201803367.
[42] T. E. Herricks, S.-H. Kim, J. Kim, D. Li, J. H. Kwak, J. W. Grate, S. H. Kim, Y. Xia, Direct fabrication of enzyme-carrying polymer nanofibers by electrospinning, *Journal of Materials Chemistry*, 2005, **15**, 3241, doi: 10.1039/b503660g.
[43] R. M. El-Shishtawy, N. S. E. Ahmed, Y. Q. Almulaiky, Immobilization of catalase on chitosan/ZnO and chitosan/ZnO/Fe_2O_3 nanocomposites: a comparative study, *Catalysts*, 2021, **11**, 820, doi: 10.3390/catal11070820.
[44] P. Katrolia, X. Liu, G. Li, N. K. Kopparapu, Enhanced properties and lactose hydrolysis efficiencies of food-grade β-galactosidases immobilized on various supports: a comparative approach, *Applied Biochemistry and Biotechnology*, 2019, **188**, 410-423, doi: 10.1007/s12010-018-2927-8.
[45] W. Z. Ng, E.-S. Chan, W. Gourich, S. H. Adiiba, M. Y. Liow, C. W. Ooi, B. T. Tey, C. P. Song, Unveiling the role of mechanical process intensifications and chemical additives in boosting lipase-catalyzed hydrolysis of vegetable oil for fatty acid production: a comprehensive review, *International Journal of Biological Macromolecules*, 2025, **284**, 138144, doi: 10.1016/j.ijbiomac.2024.138144.
[46] A. Baena, A. Orjuela, S. K. Rakshit, J. H. Clark, Enzymatic hydrolysis of waste fats, oils and greases (FOGs): Status, prospective, and process intensification alternatives, *Chemical Engineering and Processing - Process Intensification*, 2022, **175**, 108930, doi: 10.1016/j.cep.2022.108930.
[47] C. Işik, An alternative approach to plastic recycling: fabrication and characterization of rPET/CA nanofiber carriers to enhance porcine pancreatic lipase stability properties, *ACS Omega*, 2024, **9**, 31313-31327, doi: 10.1021/acsomega.3c07227.
[48] M. A. Yassin, A. A. M. Gad, A. F. Ghanem, M. H. Abdel Rehim, Green synthesis of cellulose nanofibers using immobilized cellulase, *Carbohydrate Polymers*, 2019, **205**, 255-

260, doi: 10.1016/j.carbpol.2018.10.040.
[49] P. Bayazidi, H. Almasi, A. K. Asl, Immobilization of lysozyme on bacterial cellulose nanofibers: Characteristics, antimicrobial activity and morphological properties, *International Journal of Biological Macromolecules*, 2018, **107**, 2544-2551, doi: 10.1016/j.ijbiomac.2017.10.137.
[50] Y. İspirli Doğaç, İ. Deveci, B. Mercimek, M. Teke, A comparative study for lipase immobilization onto alginate based composite electrospun nanofibers with effective and enhanced stability, *International Journal of Biological Macromolecules*, 2017, **96**, 302-311, doi: 10.1016/j.ijbiomac.2016.11.120.
[51] A. Gupta, S. R. Dhakate, M. Pahwa, S. Sinha, S. Chand, R. B. Mathur, Geranyl acetate synthesis catalyzed by Thermomyces lanuginosus lipase immobilized on electrospun polyacrylonitrile nanofiber membrane, *Process Biochemistry*, 2013, **48**, 124-132, doi: 10.1016/j.procbio.2012.09.028.
[52] J. Song, D. Kahveci, M. Chen, Z. Guo, E. Xie, X. Xu, F. Besenbacher, M. Dong, Enhanced catalytic activity of lipase encapsulated in PCL nanofibers, *Langmuir*, 2012, **28**, 6157-6162, doi: 10.1021/la300469s.
[53] F. Aspects, Nanofibrous membrane with functionalized surface, *Surface Engineering of Polmer Membranes*, 2009, 306–328, doi: 10.1007/978-3-540-88413-2_10.
[54] S.-F. Li, J.-P. Chen, W.-T. Wu, Electrospun polyacrylonitrile nanofibrous membranes for lipase immobilization, *Journal of Molecular Catalysis B: Enzymatic*, 2007, **47**, 117-124, doi: 10.1016/j.molcatb.2007.04.010.
[55] S. Nair, J. Kim, B. Crawford, S. H. Kim, Improving biocatalytic activity of enzyme-loaded nanofibers by dispersing entangled nanofiber structure, *Biomacromolecules*, 2007, **8**, 1266-1270, doi: 10.1021/bm061004k.
[56] P. Ye, Z.-K. Xu, J. Wu, C. Innocent, P. Seta, Nanofibrous poly(acrylonitrile-co-maleic acid) membranes functionalized with gelatin and chitosan for lipase immobilization, *Biomaterials*, 2006, **27**, 4169-4176, doi: 10.1016/j.biomaterials.2006.03.027.